Shielding Characteristics using an Ultrasonic Configurable Fan Artificial Noise Source to Generate Modes – Experimental Measurements and Analytical Predictions.

Daniel L. Sutliff* – *NASA Glenn Research Center, Cleveland, OH, 44212*
Bruce E. Walker† – *Channel Islands Acoustics, Camarillo, CA, 93010*

An Ultrasonic Configurable Fan Artificial Noise Source (UCFANS) was designed, built, and tested in support of the NASA Langley Research Center's 14x22 wind tunnel test of the Hybrid Wing Body (HWB) full 3-D 5.8% scale model. The UCFANS is a 5.8% rapid prototype scale model of a high-bypass turbofan engine that can generate the tonal signature of proposed engines using artificial sources (no flow). The purpose of the program was to provide an estimate of the acoustic shielding benefits possible from mounting an engine on the upper surface of a wing; a flat plate model was used as the shielding surface. Simple analytical simulations were used to preview the radiation patterns – Fresnel knife-edge diffraction was coupled with a dense phased array of point sources to compute shielded and unshielded sound pressure distributions for potential test geometries and excitation modes. Contour plots of sound pressure levels, and integrated power levels, from nacelle alone and shielded configurations for both the experimental measurements and the analytical predictions are presented in this paper.

I. Introduction

THE Subsonic Fixed Wing (SFW) and Environmentally Responsible Aviation (ERA) Projects of NASA's Aeronautics Research Mission Directorate established research goals for the development of key technologies to a readiness level of up to six (system or sub-system prototype demonstrated in a relevant environment) by the year 2020 for the N+2 timeframe. The subsonic N+2 aircraft noise level goal was set at 42 dB cumulative below the Stage 4 certification level based on a study with a set of technology assumptions configured with the innovative Hybrid Wing Body (HWB) aircraft concept[1,2]. This study used the available shielding data from a small sub-set of the data from a point noise source shielding experiment, without flow effect. In 2009, NASA and Boeing conducted a large experiment to develop the technology for jet noise shielding and to assess the shielding effect of internal engine noise sources, establishing a large database for shielding of a point noise source with flow effect[3]. This data was used in a rigorous system noise study that validated the technical approach of the earlier study to reach the 42 dB goal with the HWB aircraft concept[4].

Shielding of engine noise by airframe components has to be taken into consideration in the design of next-generation transport aircraft to meet the above noise reduction goals. Fan tones and broadband noise are important components of engine noise. Tones in particular tend to be characterized by discrete radiated modes with distinctive radiation patterns. Modeling aircraft noise accurately will depend partially on knowledge of the effect of nearby barriers on these radiation patterns. The Ultrasonic Configurable Fan Artificial Noise Source (UCFANS) is part of the larger effort mentioned above and was developed to provide a higher fidelity tonal noise source compared to the broadband point noise source used in the earlier shielding studies and, therefore, more representative of realistic fan noise sources. The purpose of this paper is to evaluate the efficacy of a simple analytical model to predict shielding and scattering of modal radiation from realistic representations of turbofan inlets and exhausts when located near finite barrier surfaces.

The UCFANS is a 5.8% percent scale model of a turbofan nacelle and fan duct used on the NASA Hybrid Wing Body (HWB). This matches the 5.8% scale model test at Langley Research Center's 14x22 wind tunnel[5]. It was designed, built, and tested for measuring acoustic shielding by prospective airframe components of modal fan tone radiation in an anechoic chamber. Artificial (no flow) noise sources are used in the model to reproduce the noise characteristics of a turbofan engine without the complexities of scaling down an operational fan. The artificial sources also offer additional control over the mode and frequency at each point in order to give a more precise database for prediction code development and validation. Model fabrication was accomplished using rapid-prototype technology at NASA Glenn Research Center.

---

* Aerospace Engineer, Acoustics Branch, 21000 Brookpark Road, MS 54-3, Associate Fellow AIAA.
† President, 676 West Highland Drive, Senior Member AIAA.

An array of 36 wide-bandwidth electrostatic actuators was installed in a dual annulus within the fan duct and driven with modally phased tone signals between 7 and 40 kHz. Three rows of 24 wide-bandwidth microphones were installed in the duct between the actuator array and the configurable inlet/exhaust exit plane to measure the modal tone generation. Modal excitation and analysis at up to nine simultaneous frequencies was accomplished by multiplexing. Note that this arrangement allows fine control over tone frequency and azimuthal mode but only limited control over radial modes.

Spectral components of the in-duct microphone data corresponding to reference excitation frequencies were spatially filtered to recover complex amplitudes of circumferential mode orders for each of the three rings. For each circumferential mode, radial components were estimated by steering vector matrix inversion for the three rings. Far-field radiation was measured using a three-dimensional traversing microphone rake. Corresponding far-field data was converted to "lossless" (spherical spreading only) levels at the locations of the microphones based on temperature and humidity data recorded for each data set[6].

The primary purpose of the program was to obtain a large database of shielding for multiple frequencies and acoustic modes at several inlet duct/wing leading edge or exhaust duct/wing trailing-edge engine radiation conditions. Earlier papers[7,8] fully documented these experimental results over multiple acoustic and geometric configurations. However, in this paper only a few select acoustic conditions with the exhaust nacelle/wing trailing-edge geometric configurations are compared to an analytical prediction method.

The analytical prediction method is similar to the Fresnel diffraction approach presented in Ahtye and McCulley[9] for point sources. A dense array of point sources was defined on an annulus representing the inlet or exhaust plane of the UCFANS model. The individual point sources were driven with appropriate amplitude and phase to represent spinning modes of specified circumferential (m) and radial (n) order. Far field sound pressures with and without a knife-edge barrier were computed as a superposition of the source-element radiation fields.

II. Analytical Prediction Methodology

Each sector was identified by its effective (ρ_0,ϕ_0,z_0) coordinate and assigned an excitation amplitude, wave-number and phase corresponding to the desired spinning mode basis function, sector area and signal frequency. Half-space free-field radiation patterns were computed to confirm the adequacy of source element density and to verify directional response reasonably consistent with classical turbofan radiation.

The calculation of point-source radiation in the presence of a half-plane barrier involves three "zones," called bright, transition and shielded. In the bright zone, the reception point is exposed to the source and its reflected image. In the transition zone, the reception point is exposed to the source but not the reflected image. In the shielded zone, the reception point is not exposed to the source. In all three zones, the reception point is exposed to the sound diffracted by the edge of the barrier. Following the method documented in Bowman, Senior and Uslenghi[10], for each element of the distributed source, the computation therefore requires a three-step process:

1. Determine the zone (bright, transition or shielded) based on the coordinates of the source element and receptor position (see Figure 1 below).
2. Compute the amplitude and phase of the signal from the possible (up to three) contributing paths
3. Add the contributing signal phasors (direct, reflected and diffracted) as applicable

Sum up the received phasors from all the source elements, convert to relative sound pressure level and phase and proceed to the next reception point.

The second step of the above process requires computation of the diffracted wave for every combination of source element and reception point, and that requires evaluation of the Fresnel integral, which can be time consuming. In order to accelerate the simulations, the relative locations of the source array, barrier edge and microphone array were pre-determined and all applicable geometrical factors were computed once and stored in a lookup table. Similarly, the Fresnel integral $F(\tau) = \int_{\tau}^{\infty} \exp(i\mu^2) d\mu$, where $\tau = \sqrt{\frac{\omega}{c}\Delta R}$ and ΔR is the length difference between the diffracted (source to barrier edge to receiver) and direct propagation paths was evaluated for a wide range of arguments and stored in a lookup/interpolate table. Figure 1 illustrates this concept, where $\Delta R = r_0 + r - R$.

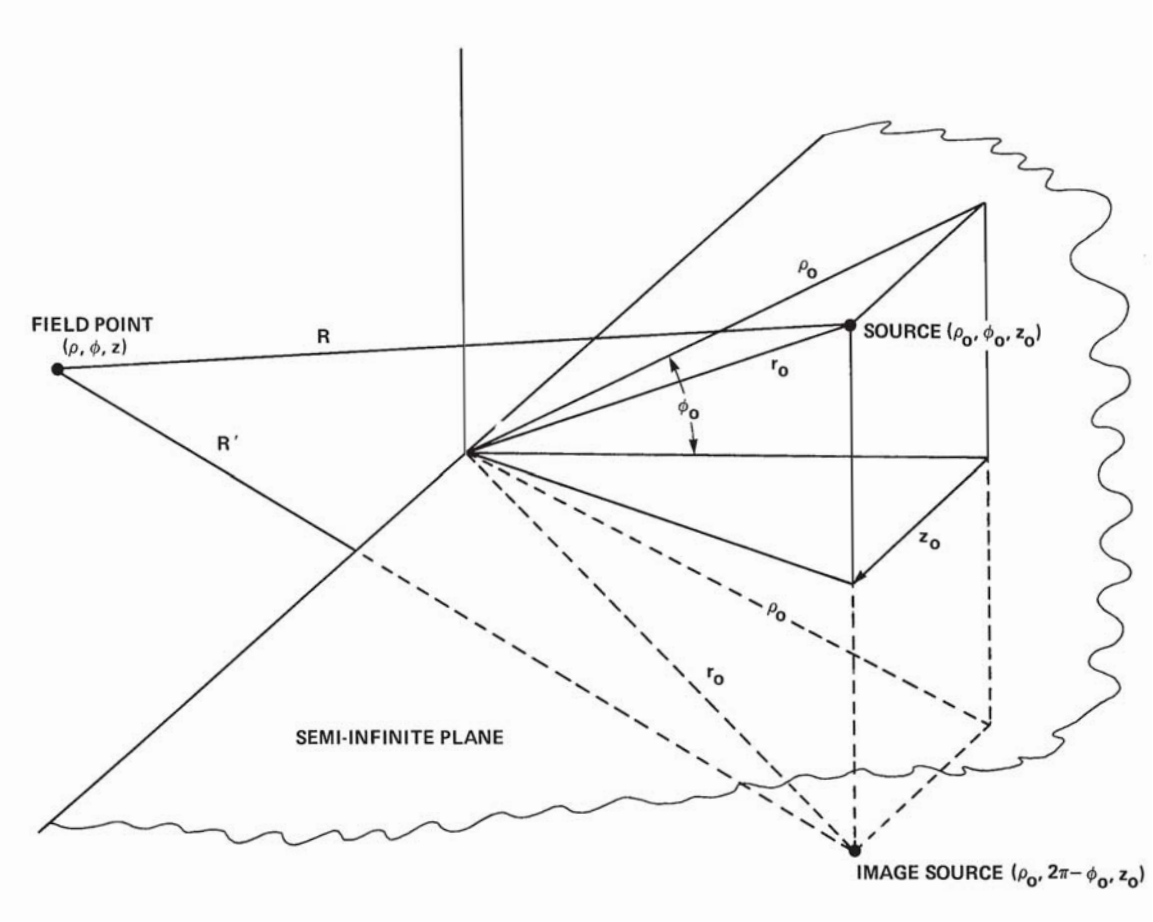

Figure 1. Illustration of coordinate system used to simulate shielding by modal source elements.

III. Experimental Facility

The Acoustical Testing Laboratory[11,12] (ATL) consists of a 23 by 27 by 20 ft (height) convertible hemi/anechoic chamber and separate sound-attenuating test support enclosure. Absorptive 34-inch fiberglass wedges in the test chamber provide an anechoic environment down to 100 Hz. A spring-isolated floor system affords vibration isolation above 3 Hz. These criteria, along with very low noise background levels, enable the acquisition of accurate and repeatable acoustical measurements on test articles that radiate very little noise. Removable floor wedges allow the test chamber to operate in either a hemi-anechoic or anechoic configuration, depending on the size of the test article and the specific test being conducted (the UCFANS test was conducted in the anechoic configuration). The test support enclosure functions as a control room during normal operations.

The measured far-field acoustic data were acquired from an array of thirteen, ¼ ” condenser style microphones. These microphones were mounted on a linear array, spaced 3” apart (resulting in a 36” span). A traverse system was utilized to move the linear array throughout the test chamber. This traverse was limited to planar motion, (e.g. a horizontal or a vertical plane, but no arcs).

IV. Test Articles

The UCFANS test article was based on the 5.8% scale model of the proposed nacelle of the N2A-EXTE HWB[5] model. This scale factor resulted in a duct diameter of approximately 6-inches, and a nacelle length of approximately 1-foot. At this scale factor the approximate full-scale relevant frequency range scaled from 400–4,000 Hz is ~ 7–70 kHz. These approximate parameters were used to guide the UCFANS design process.

The model was manufactured at the NASA Glenn Research Center using rapid prototyping methods. The ‘wing’ was limited to a 2-D planform, with the trailing and leading edge matching the contours of the HWB model, but the wing plan form was not. This was deemed an acceptable change to the 3D contour of the blended wing-body as the primary impact to scattering is concentrated near the edge, and the projected area contributes mostly to shielding.

A. Actuators

The frequency range from blade passing frequency (BPF) at approach to 3 BPF at takeoff is from just under 8 kHz to just above 57 kHz at the 5.8% model scale. To achieve this frequency range and to allow some control over radial mode content, ultrasonic electrostatic actuators were used. These actuators have a nominal frequency response of 95 dB SPL at 10 cm for a 9.9 $V_{peak\text{-}to\text{-}peak}$ 5 kHz input signal, +/- 11 dB from 4 kHz to 110 kHz. Dedicated amplifier/power supply assemblies drove the actuators.

B. Internal Microphones

The acoustic signature was measured in-duct, for modal content verification, by flush-mounted, omnidirectional electric condenser microphones. (These microphones are typically used in the audible range (20 to 16,000 Hz) but have been utilized for ultrasonic wildlife studies[13]. These microphones were evaluated for frequency response and compared to the response of a ¼” B&K 4939 style microphone. Microphones whose response was inconsistent were not used. Microphones were grouped into the three annular rings based on response measurements.

Modal separation analysis of the 3 rings of 24 in-duct microphone showed considerably more apparent scattering and aliasing than had been expected, particularly for the HWB mode set. A potential cause for this could be non-linearity in microphone amplitude response. For example, with BPF, 2BPF and 3BPF signals driving the actuators at approach conditions, the non-linear response of the microphones would result in a fictitious series of harmonics contaminating the sum and difference signals that could significantly distort the phase response at individual microphones or entire microphone rings, leading to false circumferential and radial mode identification.

C. Assembly

A drawing of the model is shown in figure 2. Areas critical to far-field acoustic radiation from the duct, such as inlet lip and duct exit dimensions were held to high fidelity, while areas not so critical to acoustics (e.g. internal flow path) were relaxed. The rapid prototype model was cast in five axial sections so that any section could be removed, replaced, or re-designed. In particular the exhaust lip and tail cone can be removed and replaced with the inlet lip and spinner to switch the model from an exhaust to an inlet radiation model. In these cases, the opposite end of the model is blocked off, and absorptive material placed in the cavity to minimize internal reflections. The remainder of the model is unchanged. The cabling for the internal drivers was routed through the center section. While this arrangement meant that the internal and external lines did not completely match the target nacelle, this area is not primarily relevant to duct/far-field radiation, and furthermore the prime objective of the test was to obtain the differences between the shielded and unshielded cases. The flexibility of this arrangement (i.e. no rewiring actuators or moving the model required to convert between the exhaust and inlet configurations), more than out weighed any

minor effect on the radiation. An appropriately scaled pylon was placed between the nacelle and wing to simulate the mounted geometry on the HWB.

D. Shield Hardware

The wing, or shield, was an aluminum plate 68.5” high that spanned the entire width of the acoustic chamber. It was decided to trade-off the 3-D plan form effects present on the HWB to concentrate on the diffraction effects of the edge. For the UCFANS in the exhaust configuration, a sharp trailing edge based on the HWB N2A-EXTE model was used. The trailing edge was made of solid rapid prototype material and was mounted on, and blended to, the aluminum plate (see figure 3a). The aft-most portion of the trailing edge part matched the N2A model lines then was blended back to the ¼” plate. For the UCFANS in the inlet condition, the edge is represented by more of the hybrid wing fuselage and was made of fiberglass. The trailing edge is affixed to the wing/wall as seen in figure 3b. Photos of the model installed in the ATL are in figure 4.

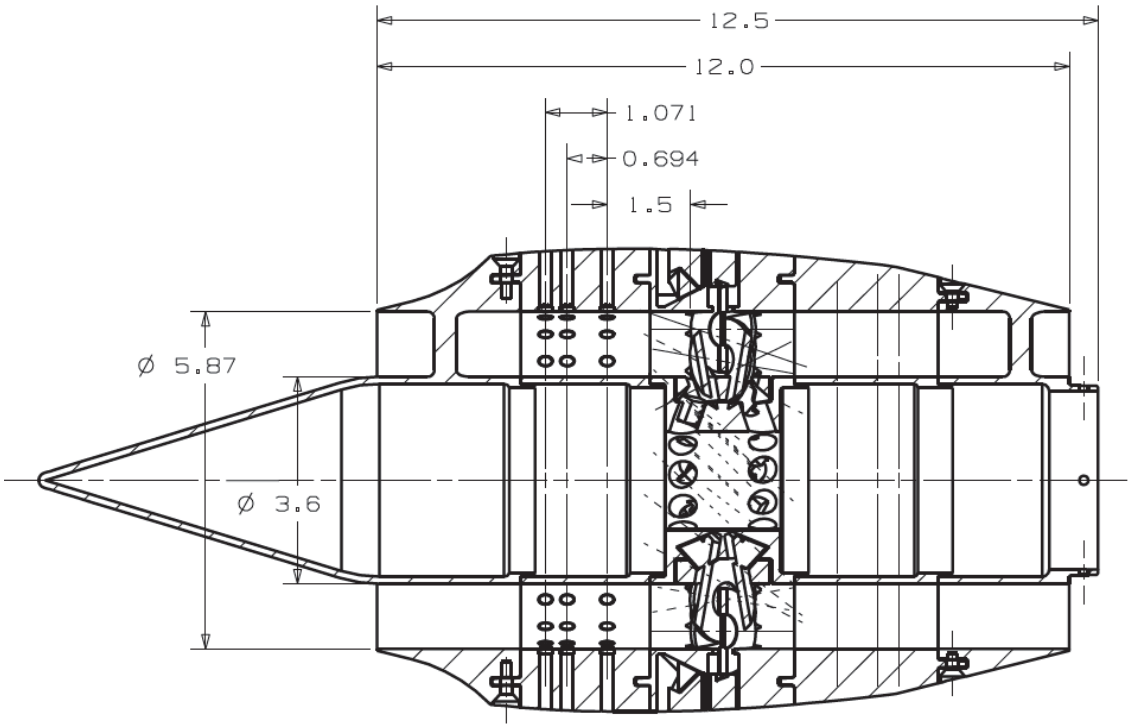

Figure 2. Line Drawing of UCFANS Nacelle in Exhaust Configuration.

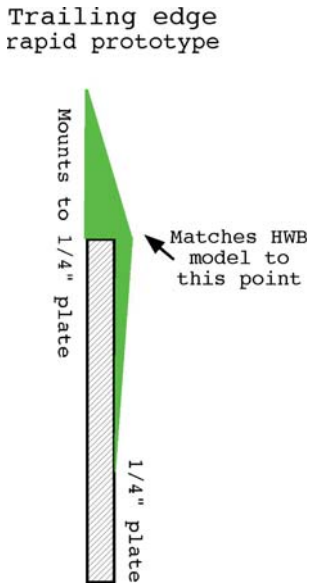

a. Trailing Edge Representation.

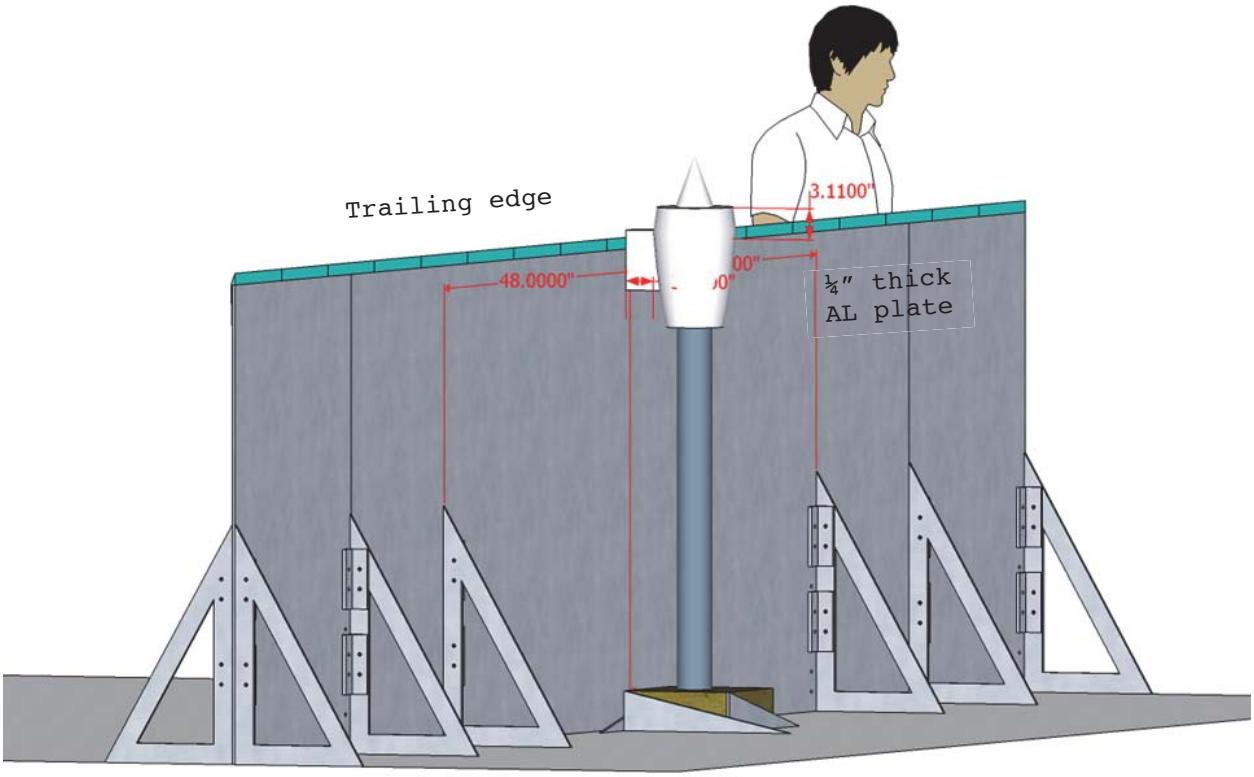

b. Trailing Edge Affixed to Wing/Wall.
(nacelle shown at the X/D=-0.5 position relative to trailing edge) .

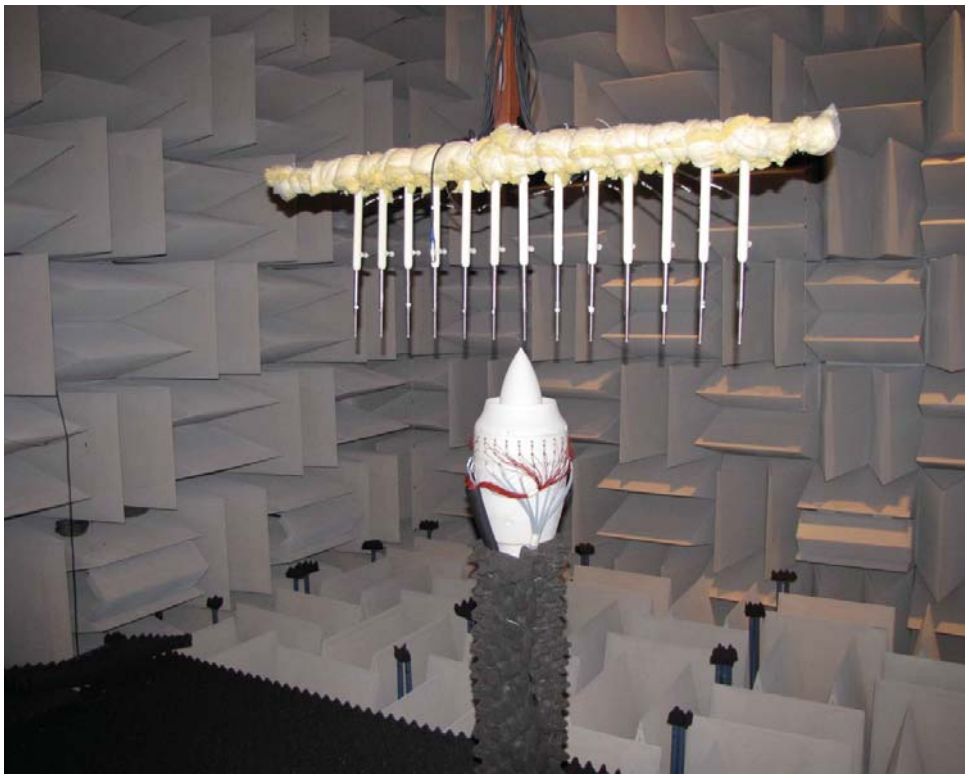

a. Isolated UCFANS Exhaust Configuration Installed in ATL.

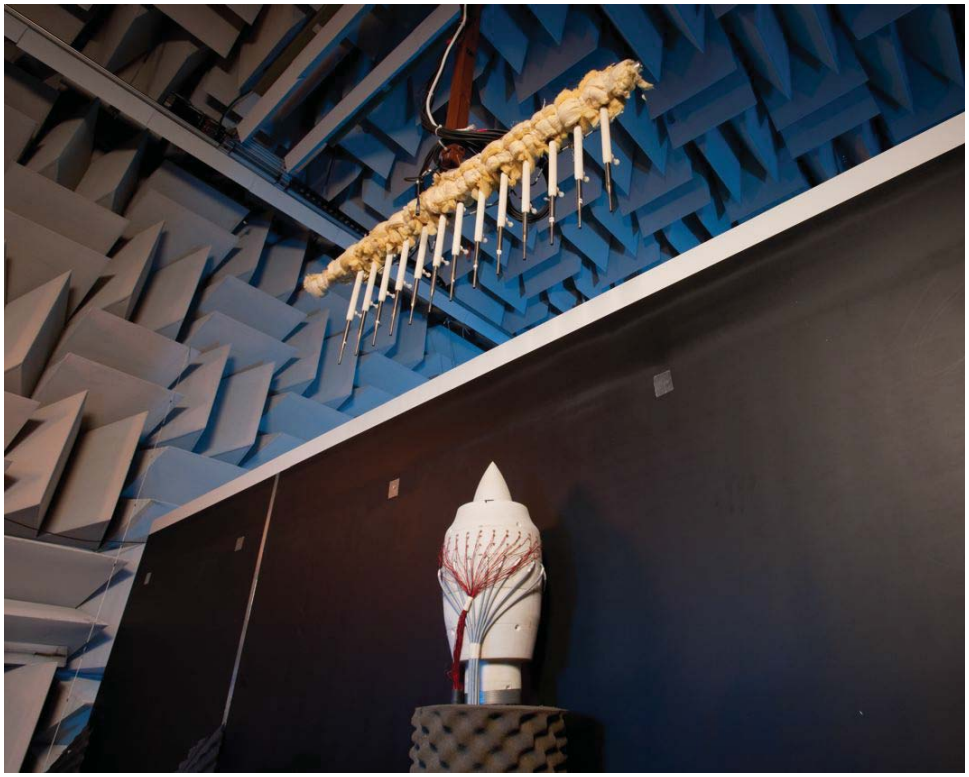

b. UCFANS Exhaust Configuration Adjacent to Shield with Trailing Edge.

Figure 4. UCFANS in Various Configurations.

E. In-Duct Signature Generation and Validation

A block diagram of the signature generation and in-duct measurement is presented in figure 5.

The signature to generate the modal content was pre-calculated using the desired modes and frequencies, and stored. Each actuator in the array was driven by a composite signal of seven excitation frequencies, equalized for variations in individual actuator amplitude and phase response, and phased to match the circumferential wave numbers of the modes to be radiated. A program created the algorithm to read in the pre-stored signal. These 36 signatures, and a reference signal were output by a 200 kS/s sample rate D/A chassis, allowing the full desired frequency range to be well below the Nyquist frequency. This reference channel consisted of the unity amplitude cosine wave of all excitation frequencies that was output directly to the data recorder. Because the test frequencies were limited to integer values up to 60 kHz, the excitation signals were multiples of one-second duration.

An additional matrix of 36, 3 second (600,000 points) Gaussian noise signals was generated applied to the test fixture actuators as an additional file. Care was taken to ensure that although the signals are statistically independent among the actuators, the radiated signal is coherent from test point to test point, allowing cross correlation and coherence computation between data taken at different traverse stops or even on different test days.

To minimize test time, 3 unique blocks of the 7 frequencies plus the broadband signature (Gaussian distribution) were generated sequentially. The two sets of radial drivers could be pre-set with a desired amplitude and/or phase relation, as a group. To achieve a variation in the radial mode generation, three consecutive, two-second signal bursts were applied with differing drive levels to the inner and outer actuators rows. Since the signal is known, parsing the frequency content from each block separately was conceptually straightforward. Effectively, this allowed for 22 separate conditions to be acquired in a short time frame.

The mode-identification microphone array consists of 72 pre-polarized condenser microphones in three rows of 24 each, allowing resolution of circumferential modes up to $|m| = 11$. The array is located approximately midway between the actuators and the duct termination, at axial positions that were determined to allow identification of radial orders $n = 0$, 1 and 2 over the BPF, and part of the 2BPF frequency range (7 to 30 kHz).

The 72 internal microphones, along with the reference signal, were acquired using an AC-coupled 200 kS/s A/D converter with integrated anti-aliasing filters. These time histories were streamed to disk for later analysis. The 72-microphone signals and a reference signal were recorded at 200 kHz sampling rate using simultaneous sampling. The cross-power spectrum of each microphone channel was computed against the reference signal and spectral components corresponding to excitation frequencies were isolated into a "compressed spectrum." The compressed spectrum for each microphone was equalized based on that microphone's calibration curve and then the 24 spectra from each microphone ring were spatially Fourier transformed to recover the complex amplitude of each circumferential mode order $-12 < m < 12$, with m=|12| measurable, but the direction indeterminate.

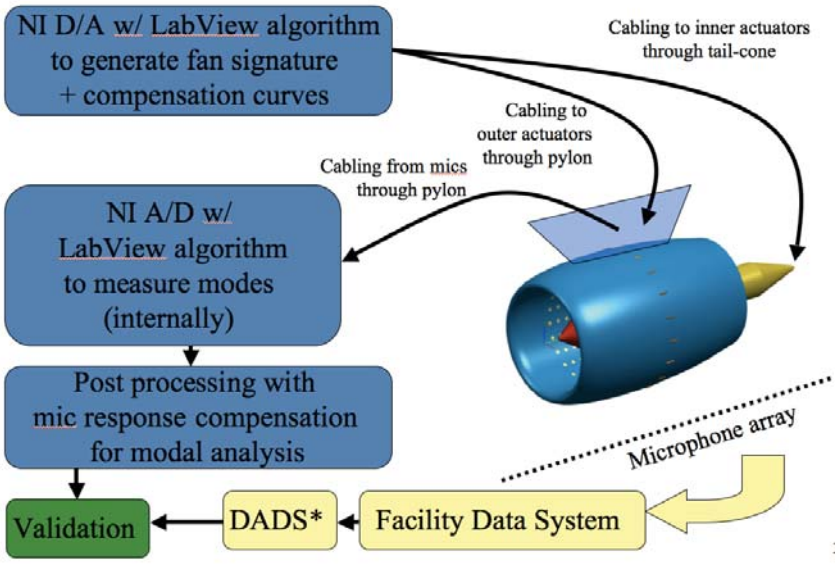

Figure 5. Block Diagram for UCFANS Signature Generation and Measurement. (*Digital Acoustic Data System)

V. Testing

A. Traverse

The general procedure was to first acquire data from the nacelle for each of the isolated (un-shielded) configurations and then repeat the data acquisition for the same geometric positions of the nacelle but with the shield installed. The far field microphone array was traversed at the same set of spatial locations for both shielded and un-shielded configurations. Thus, the nacelle configuration was tested twice, once unshielded, and subsequently with the shield in place. The nacelle height was adjusted to account for the various positions relative to the trailing edge. A key point is that the array traverse was always in the same position relative to the edge or shield, or where it would be in the case of isolated nacelle testing. Thus, the distance between the nacelle and array varied.

Acoustic time histories were acquired from a 13–microphone array. The microphone spacing on this array was 3" for a total span of 36". The 7^{th} microphone (center) at Y=0 was the position reference and tracked the model centerline. Far-field traverses were taken over four planar sweeps. Two horizontal planes were at approximately 7.5 and 10.1 nacelle diameters above the model. The two vertical planes were on one side of the model (6 and 12 diameters). The array was then shifted by 33" or 66" in the +Y or -Y direction and another planar sweep acquired. This shift resulted in overlapping data from two microphones. The total lateral span acquired was 168". The resolution between traverse stops was varied, with a finer resolution closer to the model. Figure 6a depicts the traverse plane locations relative to the model. Figure 6b illustrates the variable spacing in the Y direction of the array stops.

B. Reduced Data

A significant amount of data was acquired for HWB shielding estimates. Reported herein is a selection of the reduced data, encompassing select changes in the parametric study. The data are limited to sound pressure level (SPL) contour plots of the traverse planes. The SPL contour planes were also integrated to obtain noise power level (PWL) – (actually partial power to be used for comparison purposes). These are done for both the isolated nacelle and the nacelle with wing (shield) cases. In addition, deltas between the isolated nacelle and the nacelle + wall configurations are presented to obtain shielding values. The convention will be to denote a reduction in PWL due to shielding as a negative number (cooler colors on the contour plots). A qualitative analysis is provided herein, as the objective is to assess the character of the system. Please see references 7 and 8 for a more thorough presentation of the contour data from the full set of experimental configurations.

Far-field noise data were acquired to document the acoustic engine signature interaction with the HWB plan-form (which could be due to shielding, reflection, and diffraction) and provide data for the development of noise propagation codes. Time series data were recorded at a 200 kHz sample rate. A Kaiser window function (2^{14} points) was then applied and a Fourier transform used to convert the data to "as measured" spectra. Each spectrum was then corrected on a frequency-by-frequency basis for the individual microphone response and the effect of the grid cap (using calibration curves supplied by the manufacturer). Finally, the data were converted to a lossless condition by correcting for the atmospheric attenuation of propagating sound. Note that the data presented are at the measured planar locations and include the spherical spreading of sound. At this point, the tones of interest may be extracted from the overall spectrum.

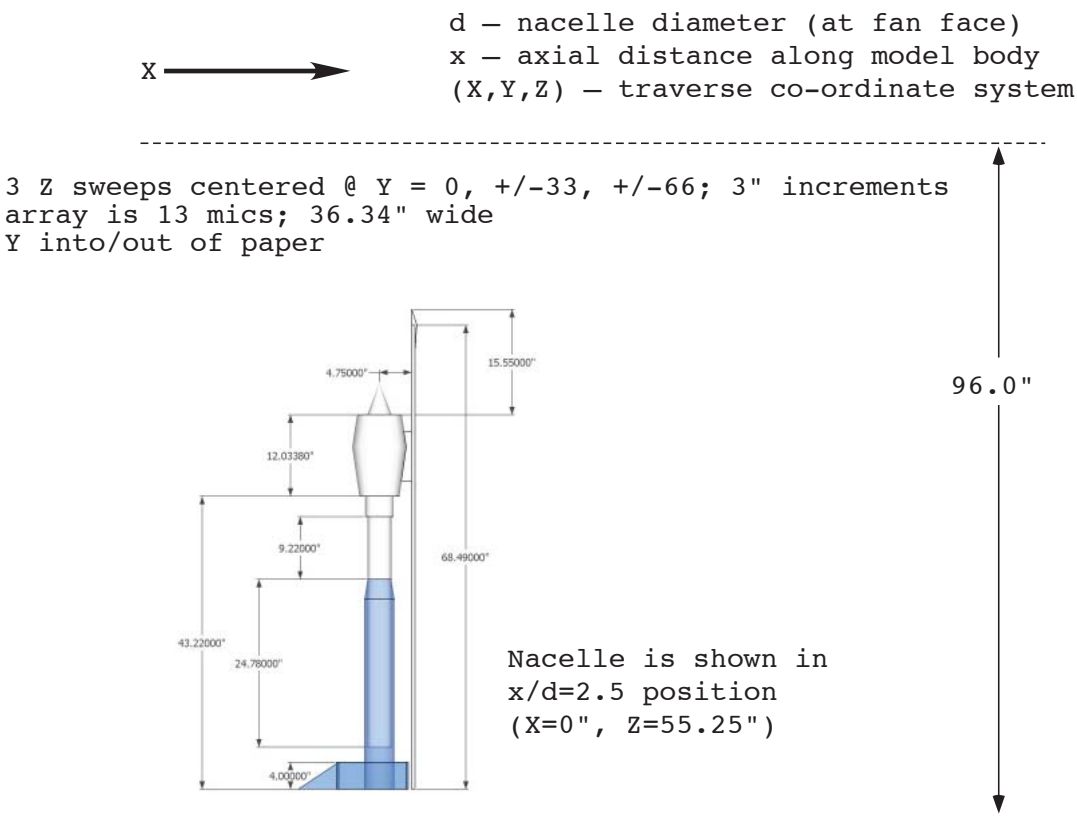

a. Traverses for Measured Acoustic Data.

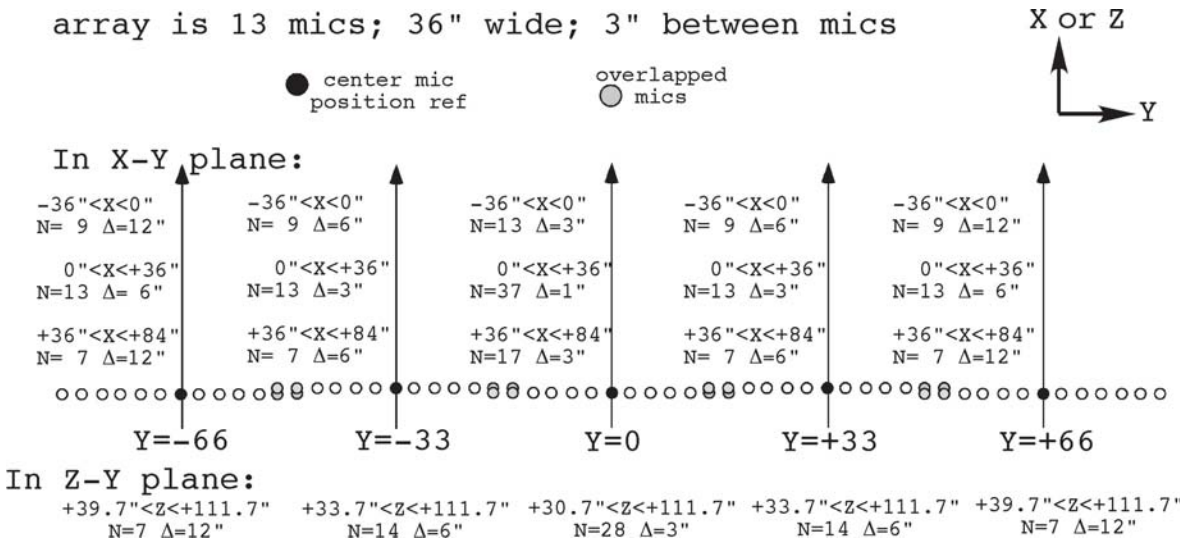

b. Resolution and spacing for X-Y and Z-Y Microphone Array Sweeps

Figure 6. Model and traverse schematic and nomenclature.

VI. Comparison of Experimental and Analytical Results

The SPL contours from the analytical predictions and measured data are plotted in figures 7 through 13. For simplicity only the exhaust configuration comparisons are presented. The contours are in a horizontal plane above the nacelle (figure 6a) and are similar for the predictions and measurements. (Keep in mind that the measured levels are absolute while the analytically predicted levels are relative.) Generally, the nacelle alone SPL contours will be on the left column, and the nacelle adjacent to the wing (wall) will be on the right column.

Figures 7 (predicted) and 8 (measured) are data from the simple mode sets acquired in reference 7. The circumferential mode generated is varied. The frequency generated was 7 kHz, which has a low modal density, so that only the n=0 radial is cut-on at each of the 3 circumferential modes. Table I provides the cut-off ratio for these modes. The SPL contours from the predicted data show the expected modal shapes from the nacelle alone with the more highly cut-on mode, m=(4,0) (fig 7a) beaming toward the centerline, and the entire lobe contained with in the measurement plane. The measured data (fig 8a) matches this distribution very well. Mode m=(6,0), having a lower cut-off ratio is more spread out since it is beamed more off-axis. The predicted (fig 7b) and measured (fig 8b) both indicate this and have similar contours. Mode m=(8,0), just barely cut-on would be expected to have a lobe missing the measurement plane. There are clear indications of that in the predicted SPL contour plot (fig 7c). The measured contour plot for m=8, (fig 8c) shows that the extraneous modes appear to bleed through at near axis.

The same generated modal conditions are presented with the wing-wall in place to provide shielding. The nacelle is at X,Y=(0,0), and the contour plane is above the nacelle, (essentially in front of the 'aircraft') one sees the reflected portion of the acoustic radiation on the left of the plot, and the 'shielded' area on the right of the plot. For modes m=4, (fig 7d & 8d) and m=6 (fig 7e & 8e) the reflected patterns match very well between the predicted and measured data contours. The striations from the reflected interference pattern match reasonably well. For m=8, the noted differences between the prediction and measured SPL contours occur, mostly likely due to the influence of the experimentally generated extraneous modes.

At the more relevant higher frequency of 14,571 Hz (which is the approach, 2BPF condition for the HWB engine) the modal structure is more complex. Mode m=-8 was generated since this matched the rotor-stator interaction mode expected from the candidate HWB engine. At this frequency up to the n=2 radial is cut-on. Due to the number of actuators (18) the generated mode is also aliased into m=10 (with up to n=1 cut-on). These limitations were necessary compromises described more fully in reference 8. Figure 9 shows the predicted radiated SPL contours for m=8 (figs 9a-c) for each radial, independently, and for m=10 (figs 9d-f). The differing and unique lobe peaks for each radial mode are clearly seen. Figure 10 shows the measured SPL contours with m=-8 generated. Experimentally, the radial content could not be explicitly controlled. Instead, recall there are two axially offset rows of circumferential drivers. Each radially offset row could be actuated independently. In figure 10a, the outer row is actuated, in figure 10b, the inner row is actuated, and in figure 10c, both rows are actuated. While the contours show a difference in the radiated patterns, it is not a direct correlation to a pure radial mode, and more interference patterns are seen, compared to the predicted analytical projections in figure 9.

Figure 11 shows the analytical prediction with m,n=(-8,0) and m,n=(10,0) superimposed to account for the aliasing in the experimentally generated modal structure (which is identified in reference 8). The interference patterns result from the interaction between the circumferential modes and tend to match the measured data better (fig 10c). The radial content of the predicted response signal was varied, but only this case is presented for brevity.

Under the assumption that modes m,n=(-8,0) and m,n=(10,0) analytically superimposed are the best match to measured data, the effect of moving the nacelle relative the trailing edge was investigated. Data from 3 positions of the nacelle were acquired (x/d = 3.14, 2.5, -0.5; defined on figure 6a). Note that x/d=2.5 is the nominal position and x/d=-0.5 has the nacelle exit located past the trailing edge by ½ of a diameter. Figure 12 shows the results from the analytical predictions for these positions for the unshielded and shielded cases, and figure 13 shows the SPL contours from the measured data for the same configurations. Qualitatively, the contours are similar for both the un-shielded and shielded cases. The x/d=2.5 shielded case has a broader reflected pattern, which may be due to a differing radial structure. At X/D=-0.5 both predicted and measured radiated patterns indicate that (as would be expected) shielding is nearly ineffective in the measurement planes.

Table I. Mode cut-off ratios

Frequency (Hz)	Mode	Cut-off ratio
7,000	(4,0)	1.95
7,000	(6,0)	1.51
7,000	(8,0)	1.01
14,571	(8,0)/(8,1)/(8,2)	2.10/1.48/1.04
14,571	(10,0)/(10,1)	1.71/1.27

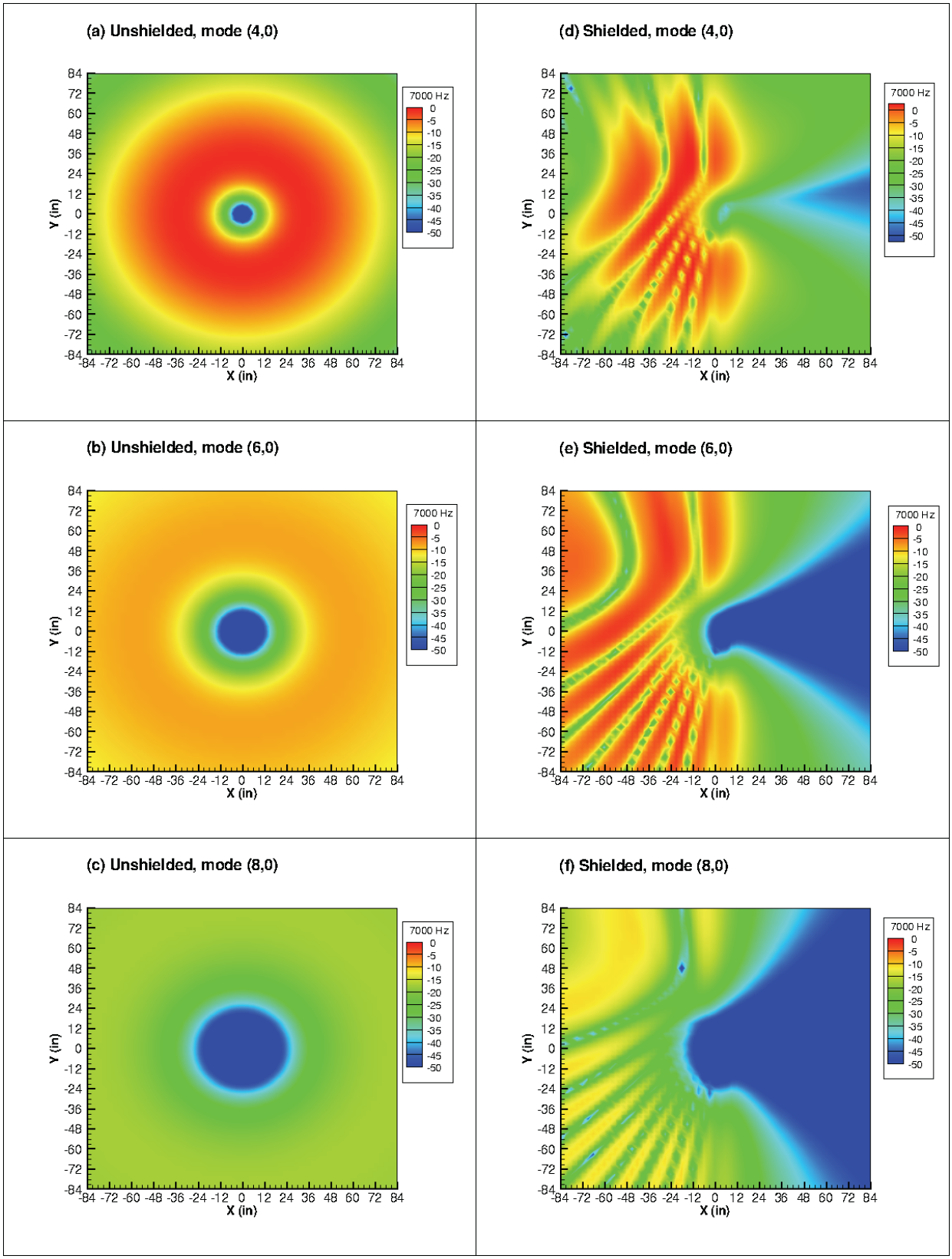

Figure 7. Predicted relative SPL contours for various circumferential mode orders. (UCFANS Exhaust Nacelle, x/d=2.5, f=7kHz)

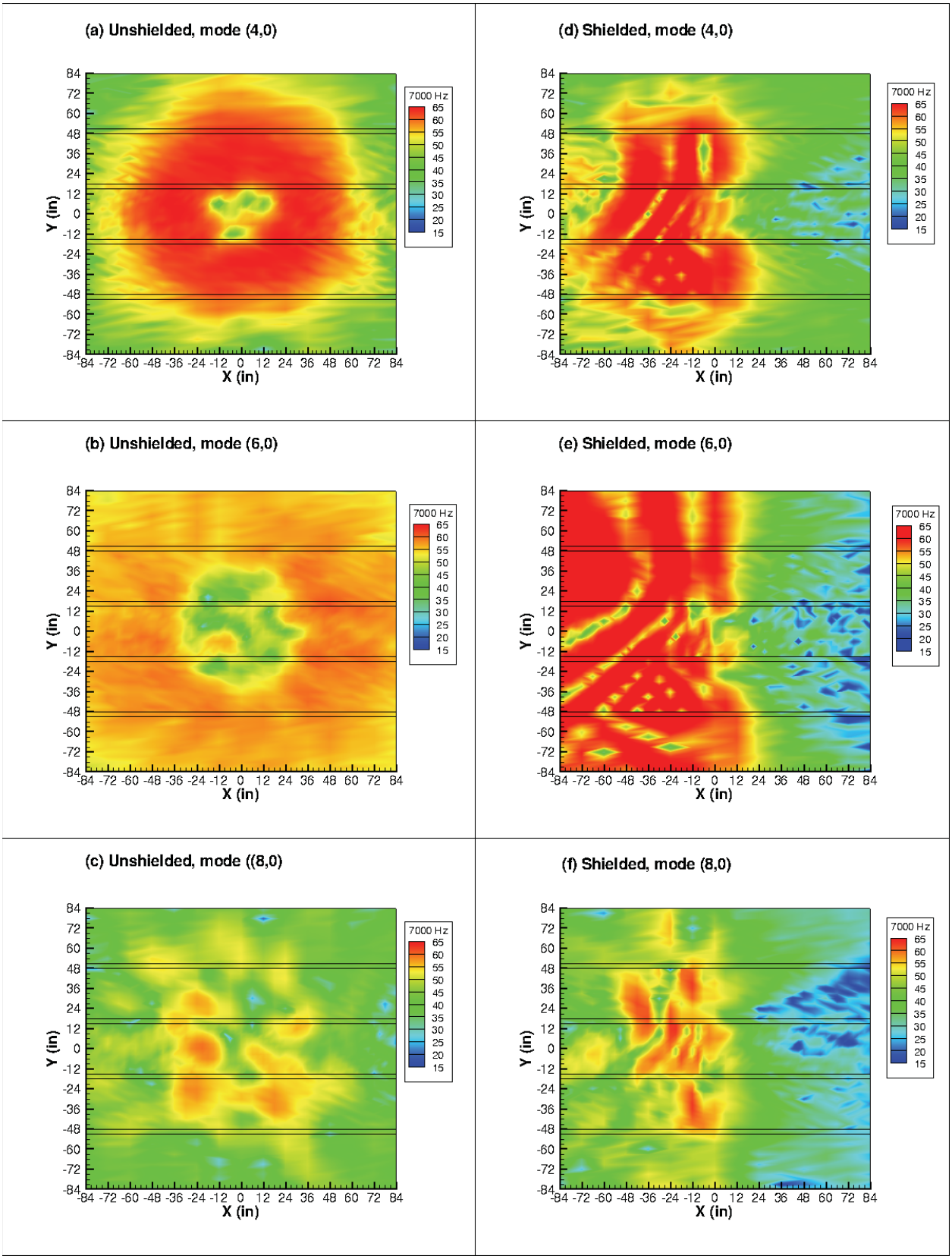

Figure 8. Measured SPL contours for various circumferential mode orders. (UCFANS Exhaust Nacelle, x/d=2.5, f=7kHz)

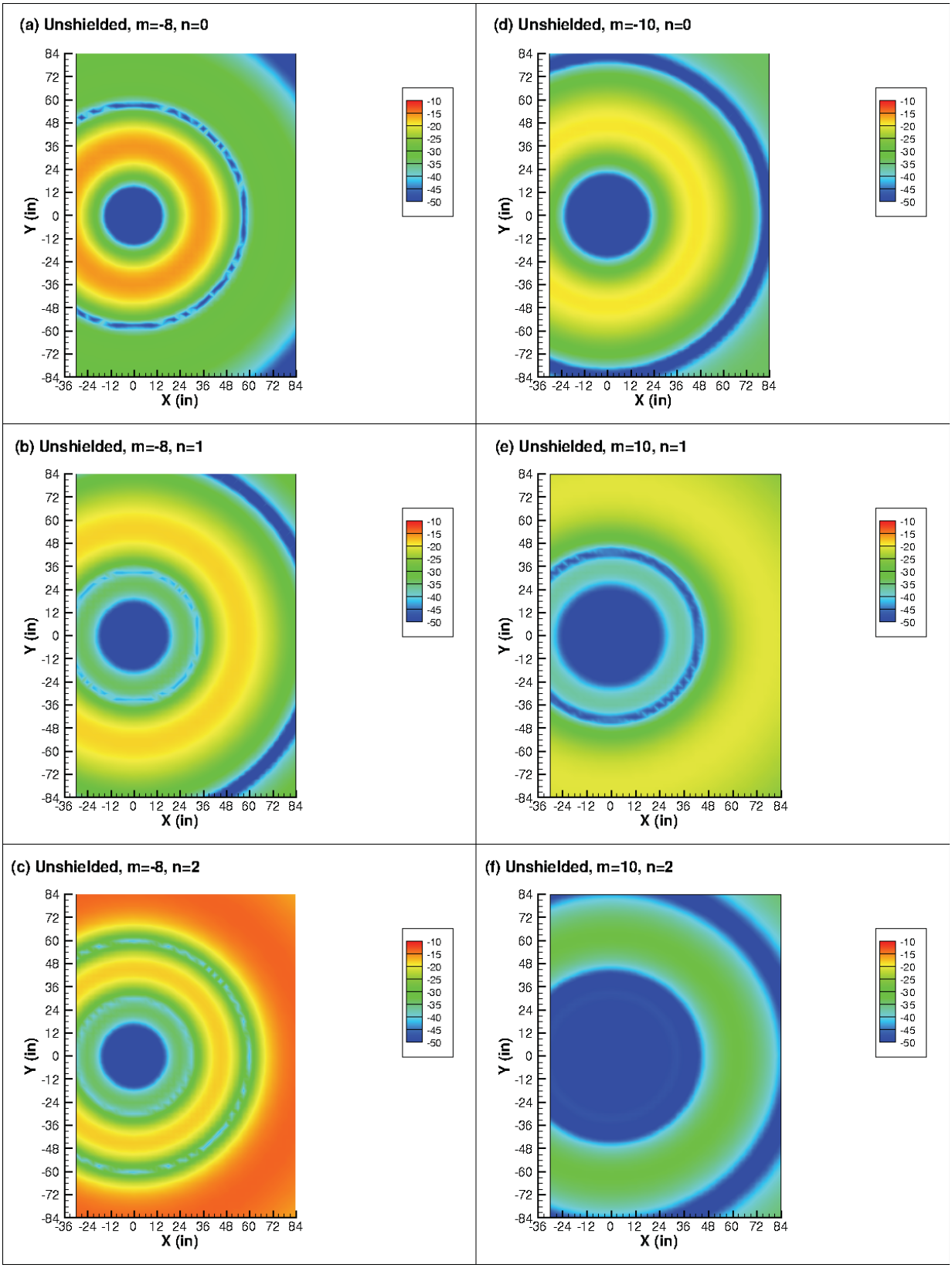

Figure 9. Predicted SPL relative contours for various circumferential mode orders. (UCFANS Exhaust Nacelle, x/d=2.5, f=14.6kHz)

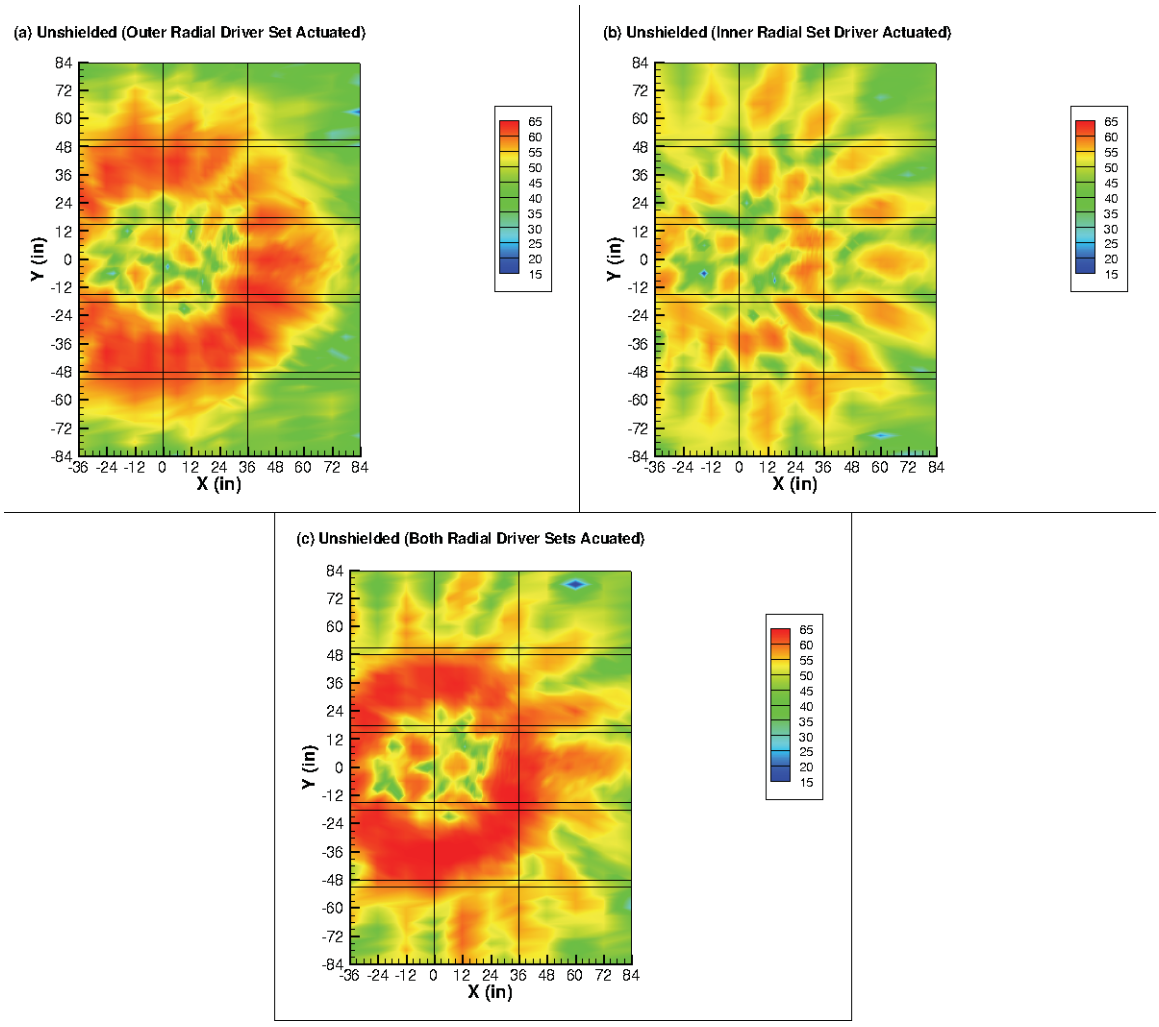

Figure 10. Measured SPL contours for various radial signals, mode m=8. (UCFANS Exhaust Nacelle, x/d=2.5, f=14.6 kHz)

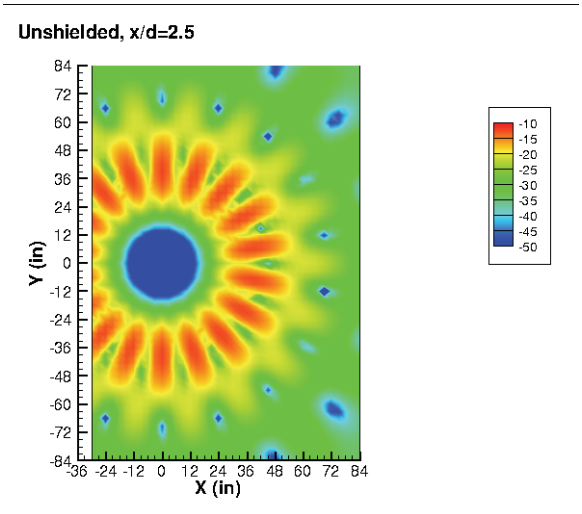

Figure 11. Predicted SPL relative contours for modes = (-8,0) and (10,0) superimposed. (UCFANS Exhaust Nacelle, x/d=2.5, f=14.6 kHz)

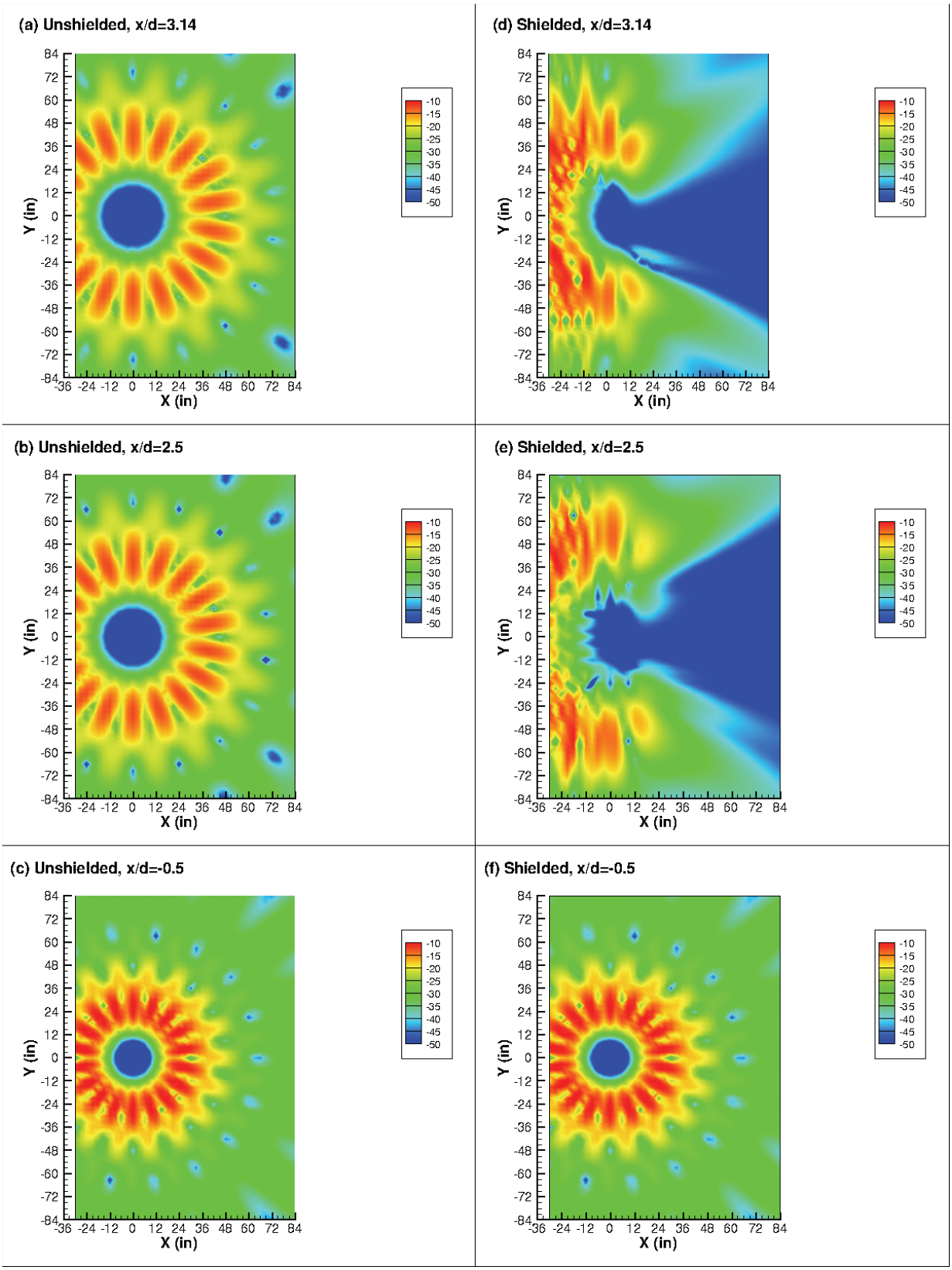

Figure 12. Predicted relative SPL contours for various nacelle positions. Circumferential modes = (-8,0) and (10,0) superimposed. (UCFANS Exhaust Nacelle, f=14.6 kHz)

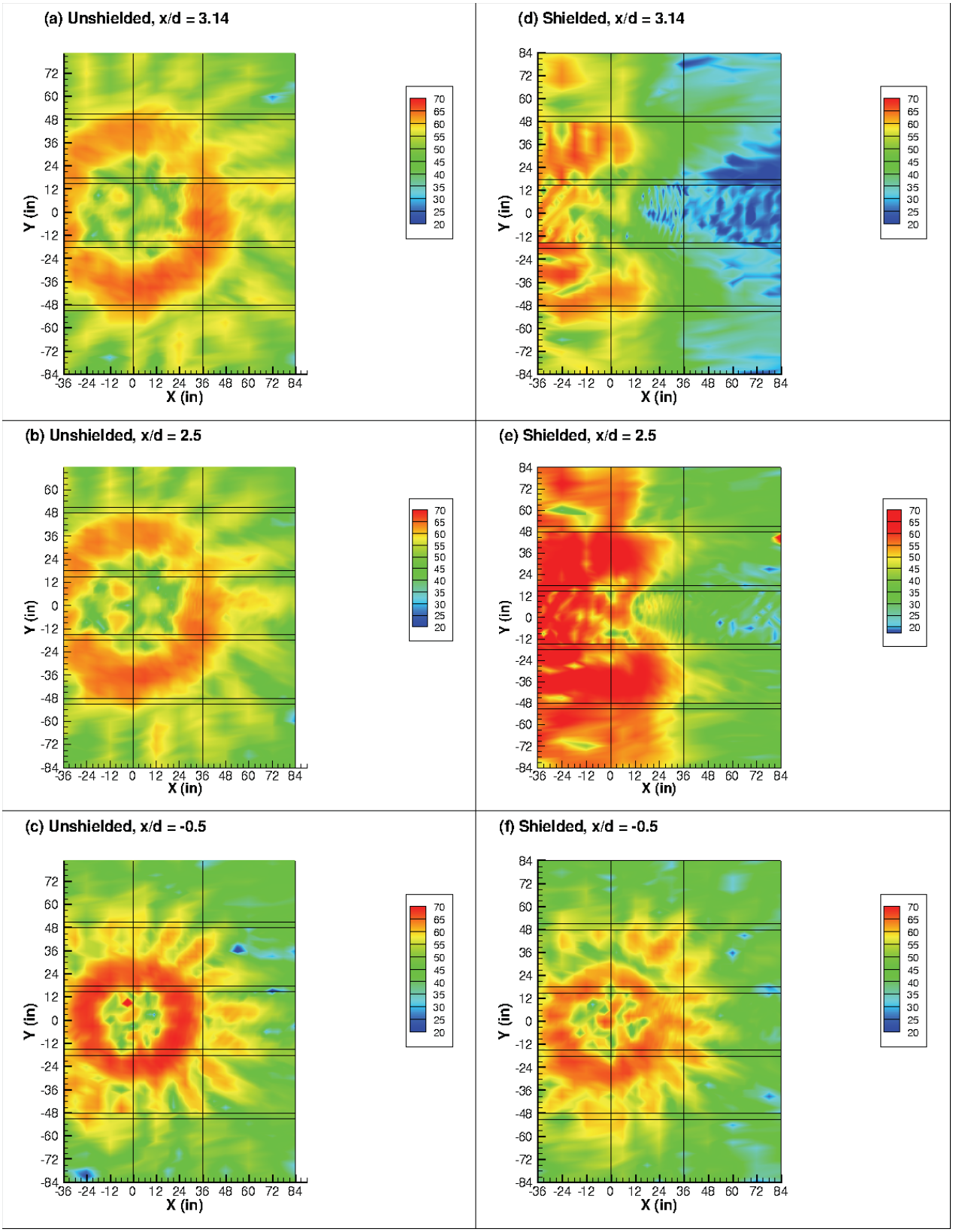

Figure 13. Measured SPL contours for various nacelle positions.
(UCFANS Exhaust Nacelle, f=14.6 kHz)

To provide some quantitative comparisons between the analytical predictions and measured radiation patterns, the PWL of the reflected side and the shielded side of the contours was computed. That is, the SPL was integrated over the partial-plane area defined by X<0 to determine the reflected PWL, and the SPL was integrated over the half-plane area defined by X>0 to determine the shielded PWL. These values were calculated for the nacelle alone and the nacelle with the wing contours. The latter was subtracted from the former to obtain the effect of the wing in these partial-planes, separately for the predictions and measurements.

Figure 14a shows these computed comparisons from the circumferential modal variations depicted in figures 7 and 8. The agreement and trends compare favorably, except for the *m*=8 shielded, which was already noted to have some extraneous modal contamination. Figure 14b shows the effect of varying the nacelle location relative to the trailing edge on the PWL. The agreement and trends also compare favorably.

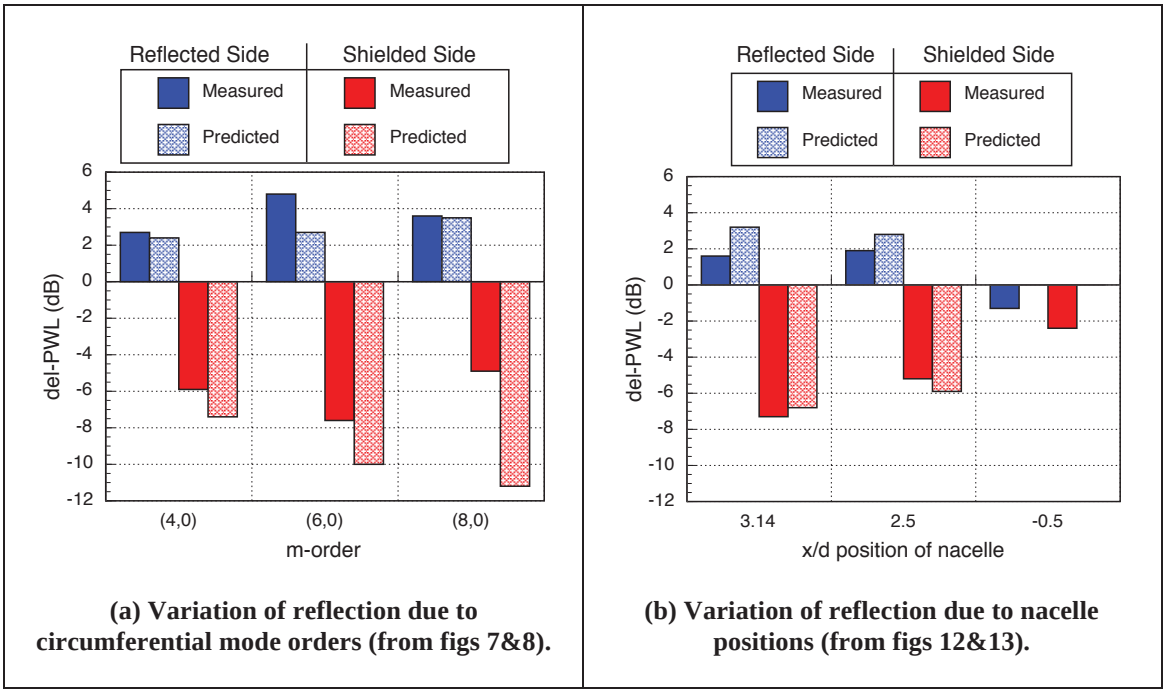

(a) Variation of reflection due to circumferential mode orders (from figs 7&8).

(b) Variation of reflection due to nacelle positions (from figs 12&13).

Figure 14. Difference in PWL in the "partial-plane" as a result of the shield installation. (PWL integrated over area X<0 – PWL integrated over area X>0).

VII. CONCLUSION

The Ultrasonic Configurable Fan Artificial Noise Source (UCFANS) test fixture is a configurable fan-mode simulator for scale model testing of engine acoustic propagation and interaction with the airframe components. The UCFANS was developed in support of the NASA Hybrid Wing Body (HWB) 5.8% scale model test at Langley Research Center's 14x22 wind tunnel and the full data sets were reported in earlier papers.

This paper presented an analytical prediction method using Fresnel knife-edge diffraction coupled with a dense phased array of point sources to compute shielded and unshielded sound pressure distributions for the geometry used in previous studies referred to through-out this paper. SPL contours and PWL computations were compared between analytical predictions and measured data. These comparisons were presented for the nacelle alone, and for the nacelle with the installed wing, configurations. Qualitatively, the SPL contours obtained from the analytical predictions and the measurements generally matched, within the limits of the modal content. Quantitatively, the effect of shielding on the PWL computations, as determined from the two data sets, agreed very well.

The simple analytical prediction method described in this paper is a useful method to predict relative SPL contours and PWL attenuation due to wing-body shielding for the purpose of parametric evaluation. More complex geometry could be explored in a future effort.

VIII. ACKNOWLEDGEMENTS

This work was supported by the NASA Integration Systems Research Program/Environmentally Responsible Aviation project and the Fundamental Aeronautics /Subsonic Fixed Wing Project.

REFERENCES

[1] Hill, G.A. and Thomas, R.H., "Challenges and Opportunities for Noise Reduction Through Advanced Aircraft Propulsion Airframe Integration and Configurations," presented at the 8th CEAS Workshop on Aeroacoustics of New Aircraft and Engine Configurations, Budapest, Hungary, Nov. 11-12, 2004.

[2] Thomas, R.H., "Subsonic Fixed Wing Project N+2 Noise Goal Summary," presentation at the NASA Acoustics Technical Working Group, December 4-5, 2007, Cleveland, OH.

[3] Czech, M.J., Thomas, R.H., and Elkoby, R., "Propulsion Airframe Aeroacoustic Integration Effects for a Hybrid Wing Body Aircraft Configuration," *International Journal of Aeroacoustics*, Vol.11, Number 3+4, 2012.

[4] Thomas, R.H., Burley, C.L., and Olson, E.D., " Hybrid Wing Body Aircraft System Noise Assessment with Propulsion Airframe Aeroacoustic Experiments," *International Journal of Aeroacoustics*, Vol. 11, Number 3+4, 2012.

[5] HWB N+2 Phase II Final Report, NASA ARMD Subsonic Fixed Wing Project, "Acoustic Prediction Methodology and Test Validation for an Efficient Low-Noise Hybrid Wing Body Subsonic Transport", NASA Contract Number NNL07AA54C, Final Report, February 2011.

[6] ANSI S1.26-1995 (R2004), "Method for the Calculation of the Absorption of Sound by the Atmosphere".

[7] Daniel L. Sutliff, Clifford A. Brown, and Bruce E. Walker, "Hybrid Wing Body Shielding Studies Using an Ultrasonic Configurable Fan Artificial Noise Source Generating Simple Modes", NASA/TM—2012-217685 also AIAA–2012-2076, Nov 2012.

[8] Daniel L. Sutliff, Clifford A. Brown, and Bruce E. Walker, "Hybrid Wing Body Shielding Studies Using an Ultrasonic Configurable Fan Artificial Noise Source Generating Typical Turbofan Modes", NASA/TM—2014-218119 also AIAA–2014-0256, Jan 2014.

[9] Warren F. Ahtye and Geraldine McCulley, "Evaluation of Approximately Methods for the Prediction of Noise Shielding by Airframe Components", NASA TP-1004, January, 1980

[10] John L. Bowman, Thomas B. Senior, and Piergiorgio L Uslenghi, editors, "*Electromagnetic and Acoustic Scattering by Simple Shapes*", Chapter 8.

[11] Beth Cooper, Alan Eckel, Trent Butcher, and David Nelson, "New Acoustical Testing Laboratory at NASA," Sound & Vibration. Dec. 2000: 10-18.

[12] Devin M. Podboy, Juilius H. Mirecki, Bruce E. Walker, and Daniel L. Sutliff, "Recent Improvements to the Acoustical Testing Laboratory at the NASA Glenn Research Center", NASA/TM—2014-218110 also AIAA–2014-0721, Jan 2014.

[13] http://www.wildlife-sound.org/equipment/technote/micdesigns/ultrasonic.html, accessed 27-October, 2011.